

Coacervation of Cationic Gemini Surfactant with Weakly Charged Anionic Polyacrylamide

Manli Deng, Meiwen Cao, and Yilin Wang*

Key Laboratory of Colloid and Interface Science, Institute of Chemistry, Chinese Academy of Sciences, Beijing 100190, People's Republic of China

Received: April 10, 2009; Revised Manuscript Received: May 31, 2009

Coacervation of cationic gemini surfactant hexamethylene-1,6-bis(dodecyldimethylammonium bromide) ($C_{12}C_6C_{12}Br_2$) with 10% hydrolyzed polyacrylamide (PAM) has been observed and investigated by turbidity titration, isothermal titration calorimetry, dynamic light scattering and microscopy. Without any assistant additive, the coacervation takes place at very low surfactant concentration, and exists in a broad surfactant concentration range. The morphology of the coacervate sponge phase varies in pore size as a function of $C_{12}C_6C_{12}Br_2$ concentration. The polymer/surfactant aggregates grow from soluble complexes with sizes smaller than 20 nm to micrometer during coacervation, and break up into soluble complexes of about 40 nm after coacervate redissolution.

Introduction

Coacervation has drawn increasing attraction owing to its fascinating properties and widespread applications in drug delivery,^{1–3} cosmetic and food formulations.^{4,5} Coacervation is the process in which a colloidal or polymer solution separates into two immiscible liquid phases: the coacervate phase concentrated in colloidal components, and the diluted equilibrium phase. This phenomenon is generally divided into simple and complex classes.^{6–9} The former is achieved by adding salts, alcohols or other additives to single component colloid solutions. The latter takes place in solutions with at least two oppositely charged macromolecular components.

Considerable efforts have been made to understand the complicated mechanism of complex coacervation. Ranganathan et al.¹⁰ studied the associative phase behavior between anionic polyelectrolytes and cationic surfactants with elaborate phase diagrams, and found that the two-phase region enclosed by the binodal or spinodal curves is strongly dependent on the polyon charge density. Dubin and co-workers^{11–14} systematically investigated the interaction of the mixed SDS/Triton X-100 micelle with poly(diallyldimethylammonium chloride), and found that charge neutralization and appropriate size of the micelle/polyelectrolyte complexes are the key requirements for coacervation. Micelle charge density, polymer molecular weight and polymer/micelle ratio have also proven important factors for coacervation, and the adjusting of ionic strength is found to be an effective approach to enhance or suppress coacervation. Generally, it has been widely accepted that coacervation is essentially dominated by a subtle balance among electrostatic, hydrophobic, and solvent interactions. However, the required balance has to be achieved by adding salts or other additives, or by adjusting pH in nearly all the complex coacervation systems. Few reports have been published on complex coacervation by varying the molecular structures of the components. Thalberg et al.¹⁵ studied the phase behavior of tetradecyltrimethylammonium bromide (TTAB) with sodium hyaluronate (NaHy) in water, and concluded that the physical origin of the observed complex coacervation is a fairly strong effective

attraction between the polymer and the surfactant. Bai et al.¹⁶ pointed out that alkyl sulfate surfactants form coacervation with hydrophobically modified polyelectrolyte through attractive electrostatic and hydrophobic interactions, but the interaction characteristics vary with the length of the surfactant alkyl chain. Vanerek et al.¹⁷ studied the coacervation of a series of cationic modified polyacrylamides (cPAM) with anionic sulfonated kraft lignin (SKL), and found that the coacervate fraction increases with increasing molecular weight of cPAM, while cPAM of low molecular weight predominantly forms precipitate with SKL. In all of the above systems, either a large amount of surfactant or polymer is required to achieve coacervation or the coacervation takes place in a narrow concentration range. Since recent decades, gemini surfactants have been well-known due to their unique properties such as remarkably low critical micelle concentration (CMC) and high surface activity. Therefore, it is intriguing whether gemini surfactants could exhibit higher efficiency in coacervation with respect to conventional single chain surfactants.

In the present work, complex coacervation is observed in the mixing system of cationic gemini surfactant hexamethylene-1,6-bis(dodecyldimethylammonium bromide) ($C_{12}C_6C_{12}Br_2$) and anionic polyacrylamide (PAM) without any additives. Here, PAM is 10% hydrolyzed and thus only weakly charged. The phase behavior, size and morphology of the interaction in the $C_{12}C_6C_{12}Br_2$ /PAM system have been studied as a function of $C_{12}C_6C_{12}Br_2$ concentration. Based on these results, the interactions between $C_{12}C_6C_{12}Br_2$ and PAM in the coacervation process are discussed.

Experimental Section

Material. Gemini surfactant $[C_{12}H_{25}(CH_3)_2N(CH_2)_6N(CH_3)_2-C_{12}H_{25}]Br_2$ ($C_{12}C_6C_{12}Br_2$) was synthesized and purified according to the method of Zana et al.¹⁸ Its structure was confirmed by mass spectroscopy and ¹H NMR, and the purity was verified by elemental analysis and surface tension measurement. Polyacrylamide (PAM), 10% hydrolyzed, was purchased from Sigma. The average molecular weight determined by viscometry is approximately 200 000. The concentration of PAM is fixed at 0.5 wt % throughout this work. The pK_a value of acrylic acid

* To whom the correspondence should be addressed. E-mail: yilinwang@iccas.ac.cn.

group of this PAM is about 4.6. Then the degree of dissociation for acrylic acid group is nearly 100% at around pH 7.0 of the experimental condition. That is to say, all the 10% hydrolyzed acrylic acid groups of the PAM carry negative charges.

Turbidimetric Titration. The turbidity of the $\text{C}_{12}\text{C}_6\text{C}_{12}\text{Br}_2/\text{PAM}$ solution, reported as $100 - \% T$, was measured at 450 nm using a Brinkman PC920 probe colorimeter thermostatted at 30.0 ± 0.1 °C. Turbidimetric titration was carried out by adding equal volumes of 120 mM $\text{C}_{12}\text{C}_6\text{C}_{12}\text{Br}_2$ and 1 wt % PAM aqueous solution into a stirred solution of 0.5 wt % PAM to increase the $\text{C}_{12}\text{C}_6\text{C}_{12}\text{Br}_2$ concentration while keeping the polymer concentration constant. All measured values were corrected by subtracting the turbidity of 0.5 wt % PAM solution.

Isothermal Titration Microcalorimetry (ITC). The calorimetric measurements were taken in a TAM 2277-201 microcalorimetric system (Thermometric AB, Järfälla, Sweden) with a 1 mL stainless steel sample cell at 30.00 ± 0.01 °C. The cell was initially loaded with 0.5 mL of water or 0.5 wt % PAM solution. Each aliquot of 5 or 10 μL of concentrated surfactant solution was injected consecutively into the stirred sample cell via a 500 μL Hamilton syringe controlled by a 612 Thermo-metric Lund pump until the desired concentration range was covered. The concentration of the surfactant in the syringe is 80 mM. The interval between two injections was 10 min, which is long enough for the signal to return to the baseline. During the whole titration process of the surfactant solution into the 0.5 wt % PAM solution, the PAM concentration was kept constant by including PAM of the same concentration in the added surfactant solution. The observed enthalpy (ΔH_{obs}) was obtained by integrating the areas of the peaks in the plot of thermal power against time.

Dynamic Light Scattering (DLS). Measurements were carried out at 30.0 ± 0.1 °C with an LLS spectrometer (ALV/SP-125) which employs a multi- τ digital time correlator (ALV-5000). Light of $\lambda = 632.8$ nm from a solid-state He–Ne laser (22 mW) was used as the incident beam. The measurement was conducted at a scattering angle of 90°. All solutions made freshly were filtered through a 0.45 μm membrane filter of hydrophilic PVDF before measurements. The correlation function of scattering data was analyzed via the CONTIN method to obtain the distribution of diffusion coefficients (D) of the solutes. The apparent hydrodynamic radius (R_h) was deduced from D by the Stokes–Einstein equation $R_h = kT/6\pi\eta D$, where k is the Boltzmann constant, T is the absolute temperature, and η is the solvent viscosity, respectively.

Light Microscopy. The image of the phase separation was captured with the $\text{C}_{12}\text{C}_6\text{C}_{12}\text{Br}_2/\text{PAM}$ solution of 10 μL by light microscope (XSP-8C(8CA)) with a mounted digital camera.

Scanning Electron Microscopy (SEM). The morphology of the sample was imaged by field-emission scanning electron microscope (Hitachi S-4300). The sample was prepared by freezing a small drop of the $\text{C}_{12}\text{C}_6\text{C}_{12}\text{Br}_2/\text{PAM}$ solution on a clean silica wafer with liquid nitrogen. Immediately afterward, the frozen sample was lyophilized under vacuum at about –42 °C. Finally, a 1–2 nm Pt coating completed the sample preparation.

Results and Discussion

The variations of the turbidity (100-T%) and the observed enthalpy change (ΔH_{obs}) for the concentrated $\text{C}_{12}\text{C}_6\text{C}_{12}\text{Br}_2$ solution being titrated into the PAM solution are presented as a function of the final $\text{C}_{12}\text{C}_6\text{C}_{12}\text{Br}_2$ concentration (C) in Figure 1A and Figure 1B. For comparison, the corresponding dilution enthalpy curve of the concentrated $\text{C}_{12}\text{C}_6\text{C}_{12}\text{Br}_2$ solution being

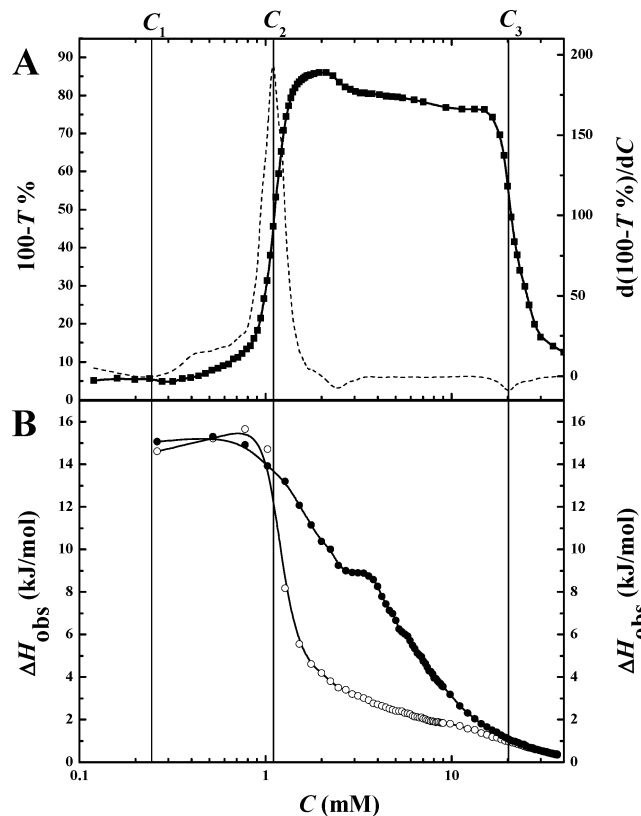


Figure 1. (A) Turbidity curve of the concentrated $\text{C}_{12}\text{C}_6\text{C}_{12}\text{Br}_2$ micelle solution titrated into 0.5 wt % PAM, and (B) calorimetric curves of the concentrated $\text{C}_{12}\text{C}_6\text{C}_{12}\text{Br}_2$ micelle solution titrated into water (open circle) and 0.5 wt % PAM (filled circle) as a function of the final surfactant concentration. The dashed line in (A) is the differentiation of the turbidity curve.

titrated into water without PAM is also included in Figure 1B, which has an approximately sigmoidal shape with an inflection point, corresponding to the CMC of $\text{C}_{12}\text{C}_6\text{C}_{12}\text{Br}_2$ (0.93 mM). From the differentiation of the turbidity curve, as demonstrated with the dashed line in Figure 1A, three critical points (C_1 , C_2 and C_3) could be identified.¹⁹ C_1 is determined as the concentration where the differential curve starts to increase from zero. C_2 and C_3 are respectively the concentrations at the maximum and the minimum of the differential curve, showing the abrupt changes in turbidity.

Below C_1 , the mixed $\text{C}_{12}\text{C}_6\text{C}_{12}\text{Br}_2/\text{PAM}$ solution is transparent, and the turbidity is very low and nearly constant. At this period, the ΔH_{obs} curve of $\text{C}_{12}\text{C}_6\text{C}_{12}\text{Br}_2/\text{PAM}$ is also close to that of the $\text{C}_{12}\text{C}_6\text{C}_{12}\text{Br}_2$ demicellization. No perceivable interaction between $\text{C}_{12}\text{C}_6\text{C}_{12}\text{Br}_2$ and PAM occurs. Increasing the $\text{C}_{12}\text{C}_6\text{C}_{12}\text{Br}_2$ concentration to C_1 , the turbidity starts to increase (as signaled by the deviation of the turbidity differential curve from zero), suggesting that the complexation of $\text{C}_{12}\text{C}_6\text{C}_{12}\text{Br}_2$ with PAM commences. Upon further addition of $\text{C}_{12}\text{C}_6\text{C}_{12}\text{Br}_2$ to C_2 , the solution starts to become quite cloudy. The turbidity drastically increases to a very high value and keeps until C_3 . Oily droplets are observed under light microscopy for the turbid solution between C_2 and C_3 , as presented in Figure 2. The suspension of the oily droplets laid in quiescence gradually separates into two transparent layers, and the viscous coacervate coagulates at the bottom. This proves that the liquid–liquid phase separation, i.e. coacervation, appears in this concentration range, so C_2 can be called the starting point of coacervation. In this region, the ΔH_{obs} curve of $\text{C}_{12}\text{C}_6\text{C}_{12}\text{Br}_2/\text{PAM}$ starts to decrease and deviate from the dilution curve of $\text{C}_{12}\text{C}_6\text{C}_{12}\text{Br}_2$.

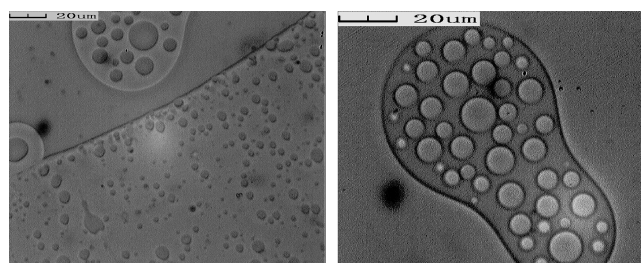


Figure 2. $\text{C}_{12}\text{C}_6\text{C}_{12}\text{Br}_2/\text{PAM}$ coacervate droplets imaged at 6.0 mM $\text{C}_{12}\text{C}_6\text{C}_{12}\text{Br}_2$ by light microscopy.

beyond C_2 , and finally joins the latter again at C_3 . The deviation of the ΔH_{obs} curve of $\text{C}_{12}\text{C}_6\text{C}_{12}\text{Br}_2/\text{PAM}$ from the dilution curve of $\text{C}_{12}\text{C}_6\text{C}_{12}\text{Br}_2$ can be attributed to the interaction of $\text{C}_{12}\text{C}_6\text{C}_{12}\text{Br}_2$ with PAM as well as the phase behavior in the mixed $\text{C}_{12}\text{C}_6\text{C}_{12}\text{Br}_2/\text{PAM}$ system. The more endothermic value of ΔH_{obs} is caused by the compensation of the $\text{C}_{12}\text{C}_6\text{C}_{12}\text{Br}_2$ aggregation with PAM to the demicellization of the added $\text{C}_{12}\text{C}_6\text{C}_{12}\text{Br}_2$ micelles. Between C_2 and C_3 , a very short flat period exists around 3.0 mM $\text{C}_{12}\text{C}_6\text{C}_{12}\text{Br}_2$ in the ΔH_{obs} curve of $\text{C}_{12}\text{C}_6\text{C}_{12}\text{Br}_2/\text{PAM}$, which suggests that the coacervation might keep the same extent with the addition of the surfactant micelles. Beyond C_3 , the turbidity significantly decreases to a low value and the two-phase mixture turns into clear homogeneous solution again. The coincidence of the ΔH_{obs} curve of $\text{C}_{12}\text{C}_6\text{C}_{12}\text{Br}_2/\text{PAM}$ with that of $\text{C}_{12}\text{C}_6\text{C}_{12}\text{Br}_2$ itself suggests that the further added $\text{C}_{12}\text{C}_6\text{C}_{12}\text{Br}_2$ does not interact with PAM anymore and the coacervate phase is completely redissolved. Consequently, the interval between C_2 and C_3 is the coacervation regime. In other words, the coacervation occurs at very low $\text{C}_{12}\text{C}_6\text{C}_{12}\text{Br}_2$ concentration and lasts in a very broad $\text{C}_{12}\text{C}_6\text{C}_{12}\text{Br}_2$ concentration range. The critical concentrations determined by the two techniques are in reasonable agreement considering the experimental errors.

Due to the poor resolution, the images of light microscopy can only show the coexistence of the two immiscible liquid phases macroscopically. DLS is employed to get further microscopic insight into the variation in size of the $\text{C}_{12}\text{C}_6\text{C}_{12}\text{Br}_2/\text{PAM}$ aggregates with the change of the phase behavior. Figure 3 shows the R_h distribution of the $\text{C}_{12}\text{C}_6\text{C}_{12}\text{Br}_2/\text{PAM}$ aggregates at the $\text{C}_{12}\text{C}_6\text{C}_{12}\text{Br}_2$ concentrations of 0 mM, 1.0 mM, 2.0 mM, 3.0 mM, 6.0 mM, and 40 mM. In the absence of $\text{C}_{12}\text{C}_6\text{C}_{12}\text{Br}_2$, PAM is polydisperse with a mean R_h of 10 nm. When $\text{C}_{12}\text{C}_6\text{C}_{12}\text{Br}_2$ is added up to 1.0 mM in the concentration region of $C_1 < C < C_2$, the average size of the aggregates is around 70 nm with a very broad distribution. The increase of R_h indicates the formation of the $\text{C}_{12}\text{C}_6\text{C}_{12}\text{Br}_2/\text{PAM}$ complexes. Within the coacervation region of $C_2 < C < C_3$, i.e., 2.0 mM, 3.0 mM and 6.0 mM, the broad peak splits into two separate peaks: one is slightly larger than the size of free PAM aggregate without $\text{C}_{12}\text{C}_6\text{C}_{12}\text{Br}_2$, while the other grows larger than several hundreds of nanometers. Meanwhile, we measured the supernatant of the solution at 6.0 mM after separating the coacervate by centrifugation, shown as a dash line in Figure 3. The peak of the supernatant overlaps with the left peak of the $\text{C}_{12}\text{C}_6\text{C}_{12}\text{Br}_2/\text{PAM}$ mixture. Thus, the left peaks with smaller R_h in the coacervation region may be assigned to the soluble $\text{C}_{12}\text{C}_6\text{C}_{12}\text{Br}_2/\text{PAM}$ complexes in the diluted equilibrium liquid, while the right peaks with larger R_h should correspond to the insoluble aggregates in the coacervate phase. In the coacervation region, as the surfactant concentration increases from 2.0 mM to 3.0 mM, the right peak shifts to larger R_h distribution and the intensity of left peak with smaller R_h decreases significantly, suggesting that

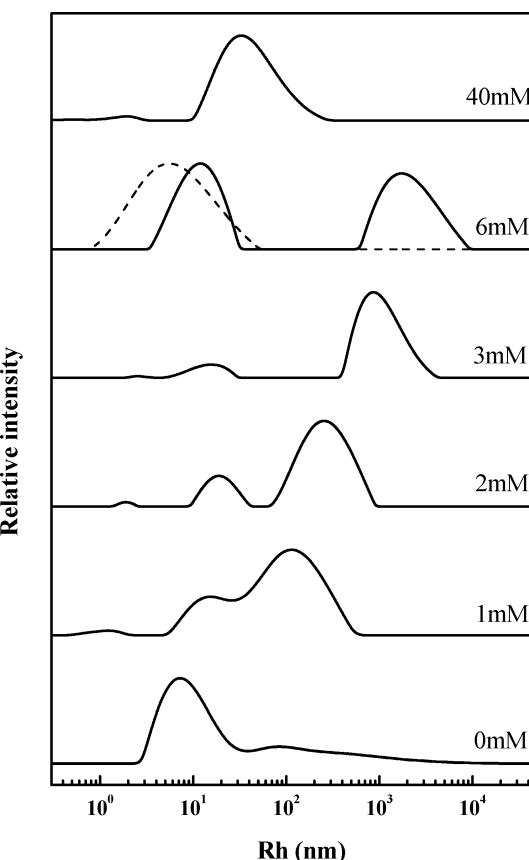


Figure 3. Distribution of the hydrodynamic radius R_h of the $\text{C}_{12}\text{C}_6\text{C}_{12}\text{Br}_2/\text{PAM}$ aggregates at different $\text{C}_{12}\text{C}_6\text{C}_{12}\text{Br}_2$ concentrations as indicated above the curves. The dashed line is the result of the supernatant separated from the mixture of 6.0 mM $\text{C}_{12}\text{C}_6\text{C}_{12}\text{Br}_2$ with 0.5 wt % PAM.

small soluble complexes grow into quite large insoluble aggregates. But with increasing the surfactant concentration from 3.0 mM to 6.0 mM, the intensity of the left peak is in turn significantly enhanced, indicating that the large aggregates partially break into soluble complexes of small sizes. It is interesting that the turning point 3.0 mM is located in the characteristic flat region of the ΔH_{obs} curve. At 40 mM, which is beyond C_3 , the R_h distribution exhibits a unimodal distribution centered at about 40 nm. Due to the disappearance of the coacervate, this size should be attributed to the redissolved $\text{C}_{12}\text{C}_6\text{C}_{12}\text{Br}_2/\text{PAM}$ complexes from the large insoluble aggregates. Apparently, the redissolved $\text{C}_{12}\text{C}_6\text{C}_{12}\text{Br}_2/\text{PAM}$ complex is much larger than the soluble complex (6–19 nm) before the coacervation region.

To have a direct observation of the morphology of the coacervate, the SEM imaging has been performed on the $\text{C}_{12}\text{C}_6\text{C}_{12}\text{Br}_2/\text{PAM}$ mixtures in the coacervation region, as shown in Figure 4. At 1.6 mM (just beyond C_2), only fibril-like alignment can be seen in Figure 4A. This could be regarded as the early stage of coacervation. At 6.0 mM, a spongelike morphology of coacervate with average pore diameter of ca. 2 μm is clearly observed in Figure 4B. The domains inside the pores are presumably occupied by the diluted equilibrium liquid phase. Similar morphology of simple coacervate formed by a zwitterionic gemini surfactant was reported by Menger's group.^{20,21} At 9.0 mM (before C_3), the network still exists but has a lower density and much larger pore sizes ranging from 10 to 60 μm , as found in Figure 4C. The fracture of the network reflects that the cross-link of the network is gradually lost during

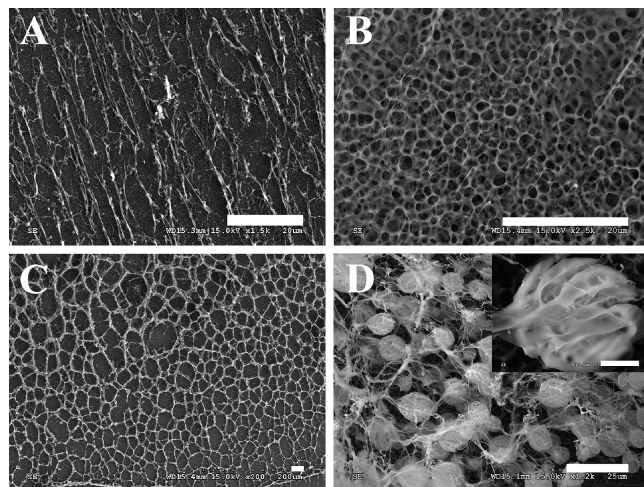


Figure 4. SEM images of the $\text{C}_{12}\text{C}_6\text{C}_{12}\text{Br}_2/\text{PAM}$ aggregates in the coacervation period formed at the $\text{C}_{12}\text{C}_6\text{C}_{12}\text{Br}_2$ concentrations of (A) 1.6 mM, (B) 6.0 mM, and (C) 9.0 mM, respectively. SEM image (D) is the $\text{C}_{12}\text{C}_6\text{C}_{12}\text{Br}_2/\text{PAM}$ aggregates in the coacervate phase at the $\text{C}_{12}\text{C}_6\text{C}_{12}\text{Br}_2$ concentration of 6.0 mM. All the scale bars represent 20 μm . The inset in (D) is the higher magnification (bar = 2 μm) of a typical stacking.

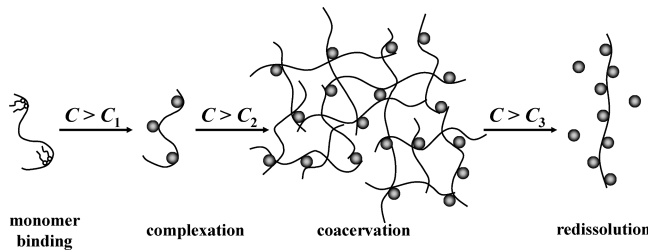


Figure 5. Schematic representation for the mechanism of the coacervation between $\text{C}_{12}\text{C}_6\text{C}_{12}\text{Br}_2$ and PAM.

the coacervate-redissolving process, where the insoluble aggregates transform into the soluble complexes which take up more space to expand the pore volume. As noted in Figure 4D, the $\text{C}_{12}\text{C}_6\text{C}_{12}\text{Br}_2/\text{PAM}$ aggregate in the coacervate phase displays quite different morphology from that of the above complexes suspending in the mixing solution. The most striking feature is the multilamellar stackings ranging from 2 to 12 μm in size. The size distribution of these aggregates in coacervate phase agrees well with the right peaks of the DLS curve at 6.0 mM in Figure 3. As reported previously,^{21,22} a phase transition from L_3 to L_α may happen, in which a coacervate converts into a simple lamellar phase. However, there are still many micro-domains occupied by water in coacervate phase. As known, one of the most obvious differences between coacervation and precipitation is the extent of dehydration in the condensed phase. Coacervate maintains a large amount of water, while precipitate is highly dehydrated.^{23,24}

Based on the above results, a simplified mechanism of the interaction process between $\text{C}_{12}\text{C}_6\text{C}_{12}\text{Br}_2$ and PAM is proposed, illustrated in Figure 5. Four stages of the $\text{C}_{12}\text{C}_6\text{C}_{12}\text{Br}_2/\text{PAM}$ interaction are involved in the mechanism, monomer binding, complexation, coacervation, and redissolution. Below C_1 , the $\text{C}_{12}\text{C}_6\text{C}_{12}\text{Br}_2$ concentration is inadequate to form micelle and its cationic monomers may bind to the oppositely charged carboxyl groups of PAM through electrostatic interaction. When the $\text{C}_{12}\text{C}_6\text{C}_{12}\text{Br}_2$ concentration is beyond C_1 , the micelle-like complexes of PAM with $\text{C}_{12}\text{C}_6\text{C}_{12}\text{Br}_2$ start to form, as reflected in the increase in turbidity and the obvious increase of aggregate size by DLS. At this stage, the cationic charges of added

$\text{C}_{12}\text{C}_6\text{C}_{12}\text{Br}_2$ micelles are much less than the anionic charges of PAM, and the $\text{C}_{12}\text{C}_6\text{C}_{12}\text{Br}_2/\text{PAM}$ complexes would carry negative net charges, which sustains their hydrophilicity and stability in solution. With increasing the $\text{C}_{12}\text{C}_6\text{C}_{12}\text{Br}_2$ concentration to C_2 , more and more charged groups of PAM are neutralized by the cationic $\text{C}_{12}\text{C}_6\text{C}_{12}\text{Br}_2$ micelles. The gradual neutralization lowers the net charge and hydrophilicity of the $\text{C}_{12}\text{C}_6\text{C}_{12}\text{Br}_2/\text{PAM}$ complexes, and reduces the repulsions between them. Thus the complexes could further associate into larger aggregates as reflected by the network in SEM images and the appearance of the right peaks in DLS curves in coacervation region. Because all the 10% hydrolyzed acrylic acid groups of PAM carry negative charges, 0.5 wt % PAM used here contains about 7.0 mM negative charges. And each $\text{C}_{12}\text{C}_6\text{C}_{12}\text{Br}_2$ molecule contains two positive charges. Thus, the charge neutralization point of $\text{C}_{12}\text{C}_6\text{C}_{12}\text{Br}_2$ with PAM should be at the $\text{C}_{12}\text{C}_6\text{C}_{12}\text{Br}_2$ concentration of around 3.5 mM, which is located in the flat region of the ITC curve, accompanied by a large amount of the insoluble complexes. In addition, the porous morphology of the coacervate reveals the higher content of water in coacervate than in precipitate. Further addition of $\text{C}_{12}\text{C}_6\text{C}_{12}\text{Br}_2$ would result in net positive charges of the $\text{C}_{12}\text{C}_6\text{C}_{12}\text{Br}_2/\text{PAM}$ complexes and a consequent electrostatic repulsion among them. Thus the network may be weakened and gradually broken up. Finally the further added $\text{C}_{12}\text{C}_6\text{C}_{12}\text{Br}_2$ exist as free micelles rather than bound micelles on PAM beyond C_3 , as reflected by the coincidence of the calorimetric binding curve with the dilution curve. The steep decline of turbidity and the small aggregate size in DLS indicate a complete redissolution of the coacervate, and the PAM backbone may be extensively stretched due to the electrostatic repulsions among the $\text{C}_{12}\text{C}_6\text{C}_{12}\text{Br}_2$ micelles on PAM.

Conclusion

Coacervation is observed in the system of cationic gemini surfactant $\text{C}_{12}\text{C}_6\text{C}_{12}\text{Br}_2$ and 10% hydrolyzed polyacrylamide PAM without any additives. The coacervation starts to occur at very low surfactant concentration and exists in a very wide surfactant concentration region. Without any additive or adjustment of medium conditions, the balance of electrostatic, hydrophobic and solvent interaction required by the coacervation is achieved by the well matched molecular structures of these two components. The obtained coacervate with sponge morphology is of tunable network density, and therefore is of promising applications in material engineering. This work helps to design and fabricate novel coacervation systems through adjusting surfactant and polymer structures.

Acknowledgment. This work is supported by National Natural Science Foundation of China, and National Basic Research Program of China (Grants 20633010, 20873158, 2005cb221300).

References and Notes

- (1) Chilkoti, A.; Christensen, T.; Mackay, J. A. *Curr. Opin. Chem. Biol.* **2006**, *10*, 652–657.
- (2) Dong, W.; Bodmeier, R. *Int. J. Pharm.* **2006**, *326*, 128–138.
- (3) Lim, F.; Sun, A. M. *Science* **1980**, *210*, 908–910.
- (4) Goddard, E. *D. J. Soc. Cosmet. Chem.* **1990**, *41*, 23–49.
- (5) Yeo, Y.; Bellas, E.; Firestone, W.; Langer, R.; Kohane, D. S. *J. Agric. Food Chem.* **2005**, *53*, 7518–7525.
- (6) Bungenberg de Jong, H. G. In *Colloid Science*; Kryut, H. R., Ed.; Elsevier: Amsterdam, 1949; pp 232–258.
- (7) Vassiliades, A. E. In *Cationic Surfactants*; Jungermann, E., Ed.; Marcel Dekker, Inc.: New York, 1970; pp 387–446.

- (8) Newton, D. W. In *Polymers for Controlled Drug Delivery*; Tarcha, P. J., Ed.; CRC Press: Boca Raton, FL, 1991; pp 67–81.
- (9) Burgess, D. J. In *Macromolecular Complexes in Chemistry and Biology*; Dubin, P., Bock, J., Davies, R. M., Schultz, D. N., Thies, C., Eds.; Springer-Verlag: Berlin, Heidelberg, 1994; pp 285–300.
- (10) Ranganathan, S.; Kwak, J. C. T. *Langmuir* **1996**, *12*, 1381–1390.
- (11) Li, Y.; Xia, J.; Dubin, P. L. *Macromolecules* **1994**, *27*, 7049–7055.
- (12) Li, Y.; Dubin, P. L.; Have, H. A.; Edwards, S. L.; Dautzenberg, H. *Macromolecules* **1995**, *28*, 3098–3102.
- (13) Li, Y.; Dubin, P. L.; Have, H. A.; Edwards, S. L.; Dautzenberg, H. *Langmuir* **1995**, *11*, 2486–2492.
- (14) Wang, Y.; Kimura, K.; Dubin, P. L.; Jaeger, W. *Macromolecules* **2000**, *33*, 3324–3331.
- (15) Thalberg, K.; Lindman, B.; Karlström, G. *J. Phys. Chem.* **1990**, *94*, 4289–4295.
- (16) Bai, G.; Nichifor, M.; Lopes, A.; Bastos, M. *J. Phys. Chem. B* **2005**, *109*, 518–525.
- (17) Vanerek, A.; van de Ven, T. G. M. *Colloids Surf., A* **2006**, *273*, 55–62.
- (18) Zana, R.; Benraou, M.; Rueff, R. *Langmuir* **1991**, *7*, 1072–1075.
- (19) Wang, Y.; Kimura, K.; Huang, Q.; Dubin, P. L.; Jaeger, W. *Macromolecules* **1999**, *32*, 7128–7134.
- (20) Peresypkin, A. V.; Menger, F. M. *Org. Lett.* **1999**, *1*, 1347–1350.
- (21) Menger, F. M.; Peresypkin, A. V.; Caran, K. L.; Apkarian, R. P. *Langmuir* **2000**, *16*, 9113–9116.
- (22) Strey, R.; Jahn, W.; Porte, G.; Bassereau, P. *Langmuir* **1990**, *6*, 1635–1639.
- (23) Hashidzume, A.; Ohara, T.; Morishima, Y. *Langmuir* **2002**, *18*, 9211–9218.
- (24) Menger, F. M.; Seredyuk, V. A.; Apkarian, R. P.; Wright, E. R. *J. Am. Chem. Soc.* **2002**, *124*, 12408–12409.

JP903326W